JACS
JOURNAL OF THE AMERICAN CHEMICAL SOCIETY

Article

pubs.acs.org/JACS

Silver-Lactoferrin Nanocomplexes as a Potent Antimicrobial Agent

Paweł Pomastowski,[†] Myroslav Sprynskyy,[†] Petar Žuvela,[‡] Katarzyna Rafińska,[†] Maciej Milanowski,[†] J. Jay Liu,[‡] Myunggi Yi,[§] and Bogusław Buszewski*[,†]

[†]Department of Environmental Chemistry and Bioanalytics, Faculty of Chemistry, Interdisciplinary Centre for Modern Technologies, Nicolaus Copernicus University, 87-100 Toruń, Poland

[‡]Department of Chemical Engineering, Pukyong National University, 365 Sinseon-ro, Nam-gu, 608-739 Busan, Korea

[§]Department of Biomedical Engineering, Pukyong National University, 45 Yongso-ro, Nam-gu, 608-737 Busan, Korea

Supporting Information

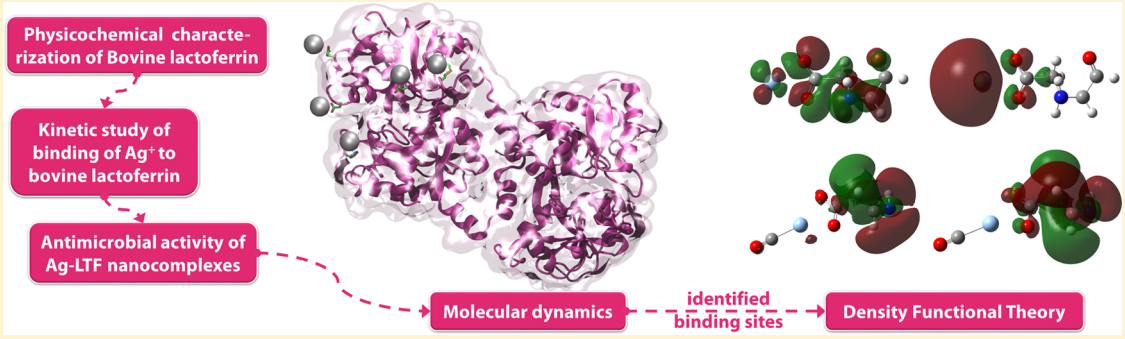

ABSTRACT: The process of silver immobilization onto and/or into bovine lactoferrin (LTF), the physicochemical properties of bovine lactoferrin and obtained silver-lactoferrin complexes, as well as antibacterial activity of silver-lactoferrin complexes were investigated in this work. Kinetic study of the silver immobilization into lactoferrin was carried out using batch sorption techniques. Spectrometric (MALDI-TOF/TOF-MS, ICP-MS), spectroscopic (FTIR, SERS), electron microscopic (TEM) and electrophoretic (I-DE) techniques, as well as zeta potential measurements, were applied for characterization of LTF and binding nature of silver in Ag-LTF complexes. On the basis of the results of the kinetics study, it was established that the silver binding to LTF is a heterogeneous process involving two main stages: (i) internal diffusion and sorption onto external surface of lactoferrin globules; and (ii) internal diffusion and binding into lactoferrin globule structure. Spectroscopic techniques combined with TEM analysis confirmed the binding process. Molecular dynamics (MD) analysis was carried out in order to simulate the mechanism of the binding process, and locate potential binding sites, as well as complement the experimental findings. Quantum mechanics (QM) simulations were performed utilizing density functional theory (DFT) in order to support the reduction mechanism of silver ions to elemental silver. Antimicrobial activity of synthesized lactoferrin complexes against selected clinical bacteria was confirmed using flow cytometry and antibiograms.

INTRODUCTION

Bovine lactoferrin (lactotransferrin, LTF) is a protein of whey and the most useful building block for the synthesis of hemoglobin, and plasma proteins. It also stimulates the proliferation of lymphocytes and phagocytic activities of macrophages.[1] LTF is an important component of the human immune system. It is a glycoprotein consisting of 689 amino-acid residues that contributes to transport and regulatory process of iron in cells. In milk, LTF occurs in the form of micelles (biocolloids). Lactoferrin biocolloids have a natural tendency for metal binding forming metalloproteins.[2] LTF is an important component of colostrum and a precursor of many bioactive peptides (e.g., Lactoferricin). LTF-derived peptides are released during enzymatic digestion. They contribute to regulatory function of organism such as hormone like-activity, opioid agonist, mineral binding, antihypertensive activity and immunomodulatory processes. Moreover, bioactive peptides of LTF can lead to cell death in sensitive pathogenic bacteria, fungi and viruses.[3] It was also reported that lactoferrin has antitumor, antiallergic and radioprotecting properties.[4]

Multidrug resistant strains of bacteria have become a serious problem in public health. The emerging resistance of bacteria and high cost of state-of-the-art antimicrobial drugs has encouraged researchers to search for effective and economically viable broad-spectrum pharmaceuticals. Therefore, the development of new potent antimicrobial compounds is crucial.[3,4]

Silver ions have accompanied people in the fight against microorganisms for hundreds of years. Even in ancient times, silver coins were used in order to inhibit fermentation of milk.[5] Nowadays, chemically and biologically synthesized silver nanoparticles are commonly used.[6] However, toxicity of free

Received: March 14, 2016
Published: June 6, 2016

DOI: 10.1021/jacs.6b02699
J. Am. Chem. Soc. 2016, 138, 7899−7909

silver cations remains a major issue. Studies showed that free silver cations cause cell membrane disruption and oxidative stress in eukaryotic cell lines. On the other hand, nanocomplexes of silver are widely used as antimicrobial, antifungal and antiviral agents and they show less cytotoxicity than silver ions on their own.[7,8] Therefore, binding the silver cations with bioactive ligands is a good approach to eliminate their toxic properties for interaction with human cells and to prevent antimicrobial attributes. Reduced cytotoxicity of silver nanoparticles end-capped by serum albumin[9] and gold nanoparticles formed in lysozyme crystals[10,11] was observed. However, the mechanism of metal ions uptake to surface of virus particles[12] and creation of ordered arrays (silver nanoparticles) on peptide nanofibers[13] are yet unclear. Hence, synthesis of silver nanocomplexes with lactoferrin represents an innovative application in the field of medicine. Along with the medicinal, bioactive lactoferrin nanocomplexes with silver (Ag-LTF) have massive potential for nutraceutical and pharmaceutical applications.

The purpose of this work was the study of the process of silver immobilization onto the protein lactoferrin. Amount of bound silver ions and physicochemical characteristics of created complexes were measured in order to verify the binding process. Molecular dynamics (MD) simulations were also performed to model the mechanism of this binding process, locate potential binding sites, and complement the experimental observations. Quantum mechanics (QM) computations were performed in order to analyze the reduction of silver. Finally, antimicrobial activity of studied nanocomplexes was evaluated, and they were compared to several commercial antimicrobial agents.

EXPERIMENTAL SECTION

Isolation of Lactoferrin. Lactoferrin was isolated from bovine whey obtained from a local dairy company (SM Drzycim, Poland). First, the whey has been diluted in a 1:1 ratio with 20 mM phosphoric buffer with 0.3 M NaCl (Sigma-Aldrich, Poland). Subsequently, the sample has been defatted in a centrifuge (8000*g*, 20 min, t = 21 °C). The clear supernatant was transferred to glass chromatographic columns with SP Sepharose fast flow (GE Healthcare, Poland) and separated in a linear gradient of 0.3−0.9 M NaCl in a 20 mM phosphoric buffer. The monitored fraction has been collected at λ = 280 nm and centrifuged at 4000*g* at 25 °C in Amicon Ultra-15 Centrifugal Filter Units (Merck Millipore, Poland) with cutoff at 30 kDa. The obtained reddish protein sample was lyophilized and frozen at −20 °C.

Electrophoretic Study. One-dimensional electrophoresis was performed using a set of Bolt Mini Gel Tank (Novex Life Technologies, Poland) gels. Reagents and samples were purchased from Novex Life Technologies, Poland and prepared according to the procedure of the manufacturer. Lactoferrin fractions were dissolved in a 50 μL Load Sample Buffer (LDS), reduced and alkylated using SampleReducing 10× agent dithiothreitol (DTT) and iodoacetamide (IAA), respectively. The samples were then heated for 10 min at 70 °C, and after stirring and cooling were applied to the gel Bolt 4−12% Bis-Tris Plus. SeeBlue Plus2 Prestained Standard was used as a marker. Electrophoretic process was carried out at 165 V during 35 min. The gels were stained for 20 min with SimplyBlue SafeStain and distained for 12 h in deionized water. Deionized water was obtained passing it through the Milli-Q RG apparatus (Millipore Intertech, Bedford, MA, USA) in our laboratory.

Isoelectric Point Determination. The isoelectric point of lactoferrin was measured using the Zetasizer Nano Series (Malvern Instruments, Malvern, Great Britain). First, the protein was suspended in a 0.09% NaCl solution (Sigma-Aldrich, Poland), and the solution was sonicated for 20 min. The suspension was titrated using 100 mM, 200 mM and 300 mM HCl solutions (Sigma-Aldrich, Poland), until the system reached a pH value of two. Finally, the titrations were carried out using 100 mM, 200 mM and 300 mM NaOH solutions (Sigma-Aldrich, Poland) to a pH of 14.

Matrix-Assisted Laser Desorption Ionization−Time-of-Flight Mass Spectrometry (MALDI-TOF/TOF-MS) Analysis. All chemicals for the MALDI-MS analyses were supplied at the highest commercially available purity by Fluka Feinchemikalien (NeuUlm, Germany; a subsidiary of Sigma-Aldrich). Ground steel targets (Bruker Daltonik, Bremen, Germany) were used for sample deposition. The α-cyano-4-hydroxycinnamic acid and sinapinic acid were employed as matrices for MALDI analysis of tryptic digest and intact proteins, respectively (dried droplet method[14]). Peptide Calibration Standard II and Protein Calibration Standards I and II (Bruker Daltoniks, Bremen) were used for external calibration. All the MS spectra were obtained using the MALDI-TOF/TOF mass spectrometer (Bruker Daltonik, Bremen, Germany) equipped with a modified neodymium-doped yttrium aluminum garnet (Nd:YAG) laser operating at the wavelength of 355 nm and frequency of 2 kHz. The system was controlled using the Bruker Daltonik software (flexControl and flexAnalysis).

LTF was dissolved in the buffer (50 mM ammonium bicarbonate ABC, pH 8.05) and incubated at 37 °C with trypsin (enzyme:substrate ratio of 1:50). Reaction was carried out at 37 °C for 14 h and terminated by the addition of 5 μL 10% TFA. Peptide mass fingerprint (PMF) spectra of tryptic digests of LTF components were recorded in reflectron positive mode, within an m/z range of 500−3500, and applying an acceleration voltage of 25 kV. Fragment spectra were determined using the LIFT post source decay (PSD) technique over an m/z range of 20−1000. MS/MS spectra were calibrated internally on immonium ions. MS spectra of intact proteins were obtained in the linear positive mode in an m/z range of 40 000−90 000, applying an acceleration voltage of 25 kV. All mass spectra were acquired and processed using dedicated software flexControl and flexAnalysis, respectively (both from Bruker Daltonik). In the case of tryptic digests of the LTF components, the obtained MS and MS/MS peak lists were submitted to a Mascot search for protein identification, with the use of BioTools and ProteinScape software (both from Bruker Daltonik), and using nonstandard search parameters, i.e., cysteine modified by carbamidomethylation. Mass tolerance was set to 0.1 Da for MS and 0.3 Da for MS/MS analysis.[14]

Batch Sorption Kinetic Experiments. Lactoferrin in a concentration of 50 mg/10 mL was suspended in 0.09% NaCl solution at pH value of six. The solution was sonicated for 5 min. 0.5 mL of LTF suspension was transferred to a 2 mL Eppendorf tube. Subsequently, 0.5 mL of a $AgNO_3$ (Sigma-Aldrich, Poland) basic solution with silver ions' concentration of 54.98 ± 0.77 mg L^{-1} was added to the tube. After incubation, the solutions were centrifuged (4 °C, 15 000 rpm, 5 min). 0.5 mL of supernatant was transferred to a Falcon probe and subjected to Millipore filtration with a molecular mass cutoff of 3 kDa and then diluted in a ratio of 1:10 with 1% HNO_3 (Sigma-Aldrich, Poland). Concentration of silver cations was determined by Inductively Coupled Plasma Mass Spectrometer, ICP-MS 7500 CX (Agilent Technologies, Japan).

The amount of silver sorption by lactoferrin from aqueous solution was determined applying the formula

$$q_t = (C_0 - C)\frac{V}{m} \quad (1)$$

where q is the amount of metal ions sorbed at a certain period of time (expressed in mg g^{-1}), m is the sorbent mass (g), C_0 is the initial concentration of silver ions in aqueous solution (expressed in mg L^{-1}), C is the concentration of silver ions in aqueous solution at certain period of time (mg L^{-1}); V is the volume of solution from which sorption occurs (L).

The sorption effectiveness at a certain period of time was calculated by the following formula:

$$E = \frac{(C_0 - C)}{C_0}100/\% \quad (2)$$

DOI: 10.1021/jacs.6b02699
J. Am. Chem. Soc. 2016, 138, 7899−7909

where E is the sorption effectiveness (expressed in %).

Sorption Kinetics Modeling. To investigate the mechanism of silver sorption by lactoferrin, several kinetic models have been applied to experimental data: zero order, pseudo-first, pseudo-second-order kinetic models and intraparticle diffusion models. The zero order kinetics model was constructed using the equation

$$C = C_0 - k_0 t \tag{3}$$

where C is the concentration of silver ions in solution at time t (expressed in mg L^{-1}), C_0 is the initial concentration of silver ions (mg L^{-1}), t is the time of adsorption duration (min), k_0 is the rate constant (mg L^{-1} min^{-1}). This model was chosen to describe the linear segments separated on the kinetic curve. The Lagergren pseudo-first-order kinetic and pseudo-second-order kinetic models[15,16] can be expressed by the equations as follows:

$$q_t = q_e(1 - e^{-k_1 t}) \tag{4}$$

$$q_t = \frac{q_e^{\,2} k_2 t}{(1 + e^{k_2 t})} \tag{5}$$

where q_e is the amount of silver sorbed at equilibrium (mg g^{-1}), q_t is the amount of metal ion adsorbed at time t (mg g^{-1}), k_1 is the rate constant of pseudo-first-order sorption kinetics (min^{-1}), k_2 is the rate constant of pseudo-second-order sorption kinetics (g mg^{-1} min^{-1}), t is the duration of sorption.

The Weber–Morris intraparticle diffusion model[17] was also applied to identify the possible mechanisms of adsorption processes, especially to calculate the rate of intraparticle diffusion, using the following equation:

$$q_t = A + K_{ip} t^{0.5} \tag{6}$$

where, q_t is the adsorbed amount at time t (mg g^{-1}), A is a constant that indicating the thickness of the boundary layer diffusion or external surface adsorption (mg g^{-1}), K_{ip} is the diffusion rate constant (mg g^{-1} $min^{-0.5}$).

Determination of Thermodynamic Parameters. The distribution coefficient (K_d) for the silver sorption by lactoferrin was calculated from the kinetic data at the equilibrium time using the equation:

$$K_d = \frac{q_e}{C_e} \tag{7}$$

where, q_e is the amount of silver sorbed by lactoferrin at equilibrium time (mg g^{-1}), C_e is the equilibrium concentrations of silver in solution (mg/L). The distribution coefficient was used as an index of adsorbent affinity to silver sorption, since a high K_d value corresponds to higher sorption capacity of sorbent, and for calculation of the change of Gibbs free energy. Therefore, the value of this coefficient was converted into a dimensionless scalar ($K_d = q_e/C_e$ = (mg g^{-1})/(mg L^{-1}) = L g^{-1} or L kg^{-1} by expressing g in kg, which is equal to kg kg^{-1}, because in this case one liter of the water solution has a density of approximately 1 kg L^{-1}).

The value of the change of Gibbs free energy ($-\Delta G^0$) for the silver sorption by lactoferrin was calculated using the following relationship:

$$\Delta G^0 = -RT \ln K_d \tag{8}$$

where $-\Delta G^0$ is the energy of adsorption in kJ mol^{-1}, R is the gas constant (8.314 J mol^{-1} K^{-1}), T is the adsorption absolute temperature in Kelvin (295 K), and K_d is the distribution coefficient.

Goodness-of-fit of the models to experimental isotherms data was evaluated using the Pearson correlation coefficient (R) and standard error (S). Accuracy of used models was determined based on the average relative approximation error (A_{approx}).

Fourier Transform Infrared Spectroscopic (FTIR) Analysis. FTIR analysis for verification of silver binding to lactoferrin has been performed. Both the native protein and Ag-LTF were suspended in 0.09% NaCl at pH 6. The infrared spectrum was measured in MIR range (FTIR Genesis II Mattson, USA) using the thin layer method on CaF_2 plates (Sigma-Aldrich, Poland). Spectroscopic data was processed using WINFIRST software.

Surface Enhanced Raman Spectroscopy Analysis (SERS). Samples were prepared in 20 μL of diH_2O, incubated for 5 h in the dark. Raman spectra were captured using a Raman Spectrometer with an optical microscope (Micro Raman 200, PerkinElmer, Poland). Spectra were obtained at the range 100–1900 cm^{-1} using a micro-Raman system in Via Renishaw. The wavelength at λ = 785 nm was used as excitation light, with the power of approximately 2 mW and the counting time spectrum at 30 s with 10 fM accumulation.

Transmission Electron Microscopy (TEM) Imaging. The size of Ag-LTF complex was measured using TEM (FEITecnai F20 X-Twintool) coupled with the Energy Dispersive X-ray (EDX), and Fast Fourier Transform (FFT) analysis (XFlash 4010 Bruker AXS). Prior to analysis, the samples have been placed on a carbon-coated copper grid (Lacey Carbon Support Film 400 mesh; Electron Microscopy Sciences) and dried at room temperature.

Molecular Dynamics (MD) Analysis. Initial structure of diferric bovine lactoferrin for MD simulations (Figure 1) was obtained from the Protein data bank (PDB) with the ID: 1BLF.[18] The structure is comprised of 689 amino-acid residues, which makes bovine lactoferrin two residues shorter than its human counterpart with which it shares 69% sequence identity.

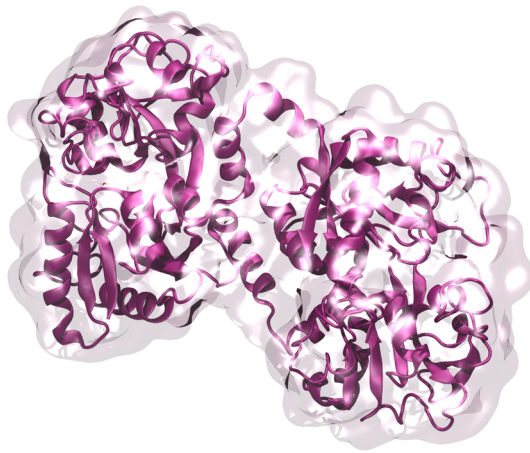

Figure 1. Initial three-dimensional structure of bovine lactoferrin used for MD simulations visualized using VMD[19] software with the ribbon representation.

NAMD 2.10[20] software with the CHARMM force field[21] was used for the MD simulations. Parameters of the CHARMM36 all-atom additive protein force field were used for all the atoms, molecules and ions except the Ag^+ and NO^{3-} ion, for which parameters were obtained from Won,[22] and the SwissParam[23] server, respectively.

Prior to running the MD simulations, the LTF was solvated in a cubic water box with a side length of 12 nm. Subsequently, the COFACTOR[24] procedure was used to predict potential binding sites. The COFACTOR procedure is based on global and local similarity search using template protein and ligand structures. Reliability of the predictions is determined using a statistical confidence score metric (C-score)[24] which is in range of values between zero and one. For the selected initial structure (1BLF) four binding sites (Table 1) with C-scores higher than 0.5 were predicted.

Although none of the predicted ligands correspond to silver cations, they were simply used as a guide for initial placement of silver cations within the lactoferrin structure for MD simulations. Additionally, 30 additional silver ions were randomly placed within the water box. The whole system was then electrically neutralized with a corresponding amount of nitrate and chloride ions in random coordinates.

Potential energy of the initial system was minimized in order to relax bonds and resolve any possible structural clashes. Periodic boundary conditions were applied according to the size of the water box. The cutoff for nonbond interactions was set to 1.2 nm with a 1

DOI: 10.1021/jacs.6b02699
J. Am. Chem. Soc. 2016, 138, 7899–7909

Table 1. Predicted Ion Binding Sites for MD Initial Structure

template	C-score	ligand	residues
1BIY[25]	0.80	CO^{3-}	341, 429, 455, 459−451, 462, 522, 591
1JW1[26]	0.75	Fe^{3+}	391, 429, 460, 522, 591
1BLF[18]	0.62	CO^{3-}	56, 88, 13, 117−120, 188, 249
1F9B[27]	0.55	3ID[a]	346, 350, 459, 515, 520−521, 633−634

[a]3*H*-indole-5,6-diol.

nm switching distance, i.e., a distance at which the switching function is utilized for their smooth truncation. The long-range electrostatic interactions were calculated by particle mesh Ewald (PMF).[28] After energy minimization, the system was gradually heated from 0 to 303.15 K using a Langevin thermostat[29] under constant volume. Subsequently, the system was equilibrated under constant pressure and temperature at 1 bar and 303.15 K, respectively. The production MD simulation was continually run for 52 ns.

Quantum Mechanical (QM) Simulation. Density functional theory (DFT)[30,31] with CAM-B3LYP functional[32] was used for QM simulations. For carbon (C), hydrogen (H), oxygen (O), and nitrogen (N), and phosphorus (P) the Pople G-31G+(d) basis set[33] was used. For the silver cation, the Los Alamos LANL2DZ[34−36] basis set was utilized. Gaussian 09W (Gaussian, Inc., Wallingford, CT, US) software was used for the computations.

First, the silver cation binding sites were pinpointed using MD simulations. Only selected protein residues and silver ions were used for QM analysis due to high computational cost. Separate QM simulations were performed for each silver binding site. Profiles of the highest occupied (HOMO) and the lowest unoccupied (LUMO) molecular orbitals were visualized using GaussView 5.0 (Gaussian, Inc., Wallingford, CT, US) in order to depict the reduction mechanism of silver.

Study of Antimicrobial Activity of Ag-LTF Complexes. Antimicrobial activity of the silver-lactoferrin nanocomplex was evaluated using flow cytometer and disc-diffusion methods as detailed in ref 37. Flow cytometry was used to evaluate the antimicrobial activity of antibiotics: vancomycin, cefotaxime, ampicillin, amoxicillin, clavulanic acid, clindamycin, metronidazole and ciprofloxacin (Sigma-Aldrich). Optical density (OD) of bacterial cultures was measured at λ = 600 nm using the BIOLOG multimode reader. Antimicrobial activity of Ag-LTF was tested against *Staphylococcus aureus* ATCC 11632, Methicillin resistant *S. aureus* MRSA (from the collection of Centre for Modern Interdisciplinary Technologies, Nicolaus Copernicus University in Toruń), *Pseudomonas aeruginosa* ATCC 27853, *Escherichia coli* ATCC 25922 and *Enterococcus faecalis* ATCC 14506.

RESULTS AND DISCUSSION

Characteristics of Lactoferrin. Lactoferrin was isolated in a phosphoric buffer at a 0.3−0.9 M NaCl linear gradient. The highest content of protein (0.283 mg mL^{-1}) was observed between 0.7 and 0.8 M NaCl. The average amount of dry lactoferrin was 61.64 ± 38.08 mg from 500 mL of whey. The content of lactoferrin in bovine milk varies between 11.08 to 493.60 mg/L.[38] An increased amount of LTF was observed in case of colostrum and mastitis. Purified lactoferrin was analyzed using electrophoresis with a 4−12% gradient. One single band of protein was observed in a range of 98−62 kDa (Figure S1). Other potential factors influencing lactoferrin content in bovine milk are various breeds (genetic diversity), lactation stage, their diet and age and as a consequence daily milk production.[39] In order to precisely determine the mass of lactoferrin, intact protein analysis using MALDI TOF MS (Figure 2A) in linear mode, was performed. Average masses of lactoferrin were in range of 77.167−81.189 kDa, which is in accordance with literature values (average mass range of 77−84 kDa[1,40]). Differences in the masses are associated with the most common form of co- and post- translation protein modification: glycolysiation. Studies have shown[40,41] that lactoferrin exhibits a degree of glycosylation changes and is associated, i.e., with stage of lactation, inflammation, environmental and stress conditions.

Content of glycan component of bovine lactoferrin can be from 6.7% to 11.2%.[41] It was reported that it is still unclear which glycan is bound to each of the glycosylation sites of bovine lactoferrin.[40] A more detailed identification was carried out after tryptic digestion, followed by analysis of the fingerprints and MS/MS spectra of selected peptides obtained in positive reflectron and LIFT modes, respectively. Mass spectra of LTF tryptic peptides are depicted in Figure 2B.

Peak lists generated on the basis of the obtained PMF spectra were subjected to a database search (SwissProt) for protein identification. PMF results were confirmed by an MS/MS search based on selected peptides (Figure 2C). Measured and theoretical masses of the detected peptides are summarized in Table 2.

Sequence coverage (SC) for lactoferrin was in a range of 19−25%. Relatively low SC results were a consequence of the nature of LTF, i.e., LTF is an iron-saturated protein, resistant to tryptic digestion.[41] Moreover, relatively high amounts of lysine (7.8%) in the structure of lactoferrin and high content of acidic amino-acids such as aspartic (5.3%) and glutamic acids (5.9%) situated near the lysine or arginine generate the missed cleavage sites.[42] Therefore, it was necessary to perform intact protein analysis combined with MS/MS of selected LTF markers for unambiguous identification of proteins.

Protein microtitration has shown that, as a function of pH (Figure 3), zeta potential (ζ) values of LTF vary from 20 to 35 mV at the pH values of 2−4. At the pH values of 4.5−11 pH, a

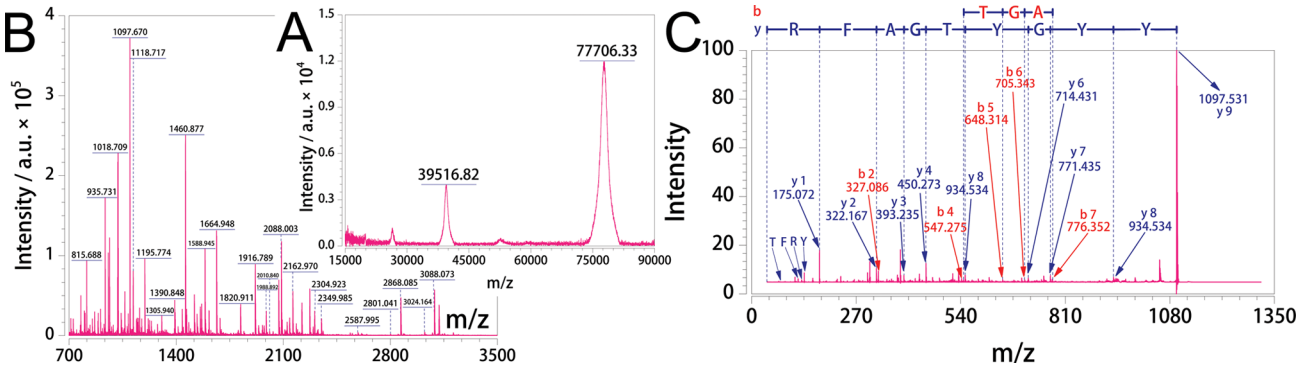

Figure 2. Mass spectrograms of (A) intact protein, peptide mass fingerprint (PMF) of (B) lactoferrin, and (C) YYGYTGAFR peptide.

DOI: 10.1021/jacs.6b02699
J. Am. Chem. Soc. 2016, 138, 7899−7909

Table 2. Spectrometric Characteristics of Lactoferrin

m/z	$[MH]^+$	residue	identified sequences[a]
831.452	831.43	13−17	RWQWR
1062.541	1062.57	14−20	WQWRMKK
2076.120	2076.10	21−39	LGAPSITCVRRAFALECIR
1590.752	1590.88	31−44	RAFALECIRAIAEK
2295.147	2294.99	40−61	AIAEKKADAVTLDGGMVFEACR
1820.991	1820.91	62−77	DPYKLRPVAAEIYGTK
1805.941	1805.77	273−288	NKSRSFQLFGSPPGQR
805.394	805.63	325−331	ETAEEVK
1664.773	1664.95	491−506	SRLCALCAGDDQGLDK
2550.211	2550.02	491−514	SRLCALCAGDDQGLDKCVPNSKEK
1097.670	1097.51	515−523	YYGYTGAFR
890.476	890.68	563−570	LLCLDGTR

[a]Peptide sequences identified based on a Mascot search.

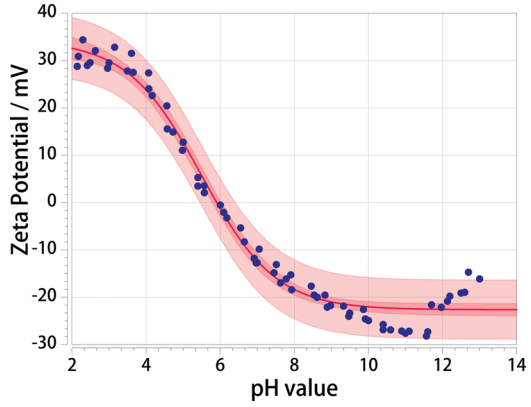

Figure 3. Zeta potential of lactoferrin as a function of pH. Confidence band is depicted in darker, whereas the prediction band is depicted in lighter pink. Red line represents the sigmoidal fit trendline.

decrease of zeta potential value from +20 to −30 mV was observed. Above pH value of 11, zeta potential decreased to −10 mV. According to Figure 3 the maximum value of zeta potential was +25 ± 0.3 mV at the pH range in between 2 and 4, as well as −30 ± 0.25 mV at pH values of 10−11.

Considering the highest absolute zeta potential value and the smallest particle size, the system reached the highest dispersion stability at the pH ranges of 2−4 and 10−11. The zero value of zeta potential was reached at pH = 6 ± 0.3.

Zeta potential analysis is a technique for determining the surface charge of biocolloids and for understanding the state of the protein surface. Additionally, it is useful for determination of the protein's isoelectric point (pI).[43] Many authors claim that the absolute zeta potential of a biological system greater than ±25 mV suggests that the particles would remain in a dispersion state for a longer period, and are not susceptible to rapid agglomeration.[44] Unfortunately, the strong acid and basic conditions cause degradation of the protein's quaternary structure which leads to loss of its biological activity. At the pH range of 2−4, strong protonation of amino-acid carboxyl and amino groups is present. Similar occurrence was observed at pH range 10−11. The system reached stability of dispersion, due to deprotonation of carboxyl groups of aspartic and glutamic acid, sulfhydryl groups of cysteine, imidazole ring of histidine and phenolic groups of tyrosine. This phenomenon is caused by the occurrence of strong repulsion and weak attractive forces between the solvated particles. The decrease of zeta potential at 4.5−10 pH is undoubtedly associated with the gradual deprotonation of active functional groups. Above the pH value of 11, an increase in ζ was observed. This increase was caused by the degradation of LTF. The isoelectric point, pI of isolated lactoferrin was 6 ± 0.3. For bovine lactoferrin, in literature pI values of 7.8 and 8.0 were obtained using free-boundary electrophoresis, while values of 4.8−5.3 were obtained by polyacrylamide gel isoelectric focusing (IEF).[45] The somewhat inconsistent pI values of bovine lactoferrin may be explained by different interaction of proteins with acid/base solvent in microtitration approach or specific nature of the carrier ampholyte interact with the lactoferrin molecule (electrophoretic methods). The isoelectric point (ζ = 0) was influenced by dissociation of functional groups, transport of ions away from the surface of the particles and the surface adsorption of ions. Consequently, charge density on the surface of proteins depends on pH, nature and concentration of added

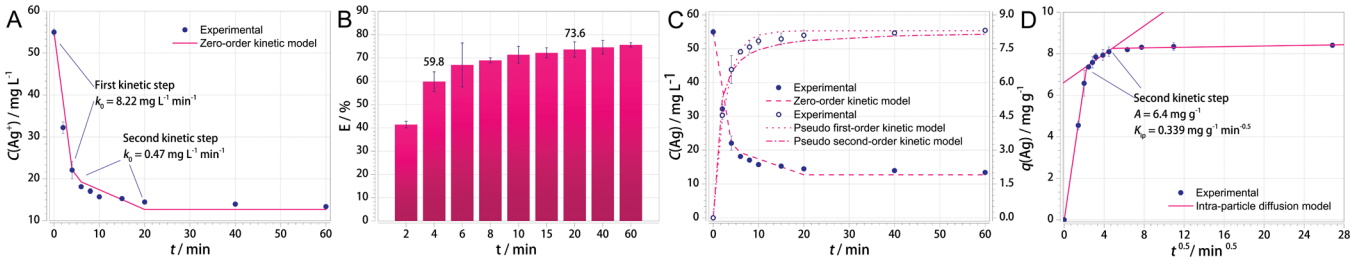

Figure 4. Kinetics of the silver onto lactoferrin sorption process. The kinetic steps of the silver ions sorption by lactoferrin and values of the rate constants determined using (A) zero order kinetic model. Subsequently, (B) represents the sorption effectiveness of the silver ions by lactoferrin, (C) experimental data and fitted pseudo-first- and the pseudo-second-order kinetics models of the silver ions sorption by lactoferrin, and (D) intraparticle diffusion model(s) plot of the silver ions sorption by lactoferrin. Error bars denote standard deviations. (n = 3).

DOI: 10.1021/jacs.6b02699
J. Am. Chem. Soc. 2016, 138, 7899−7909

Table 3. Kinetic Models' Parameters for the Silver Sorption by Lactoferrin

zero order kinetic model		pseudo-first-order kinetic model		pseudo-second-order kinetic model		intraparticle diffusion model	
First step		q_e/mg g^{-1}	8.55	q_e/mg g^{-1}	8.55	A/mg g^{-1}	6.4
k_0/mg L^{-1} min^{-1}	8.22	k_1/min^{-1}	0.377	k_2/g mg^{-1} min^{-1}	0.1062	K_{ip}/mg g^{-1} min$^{-0.5}$	0.339
Second step		S	0.1902	S	0.3367		
k_0/mg L^{-1} min^{-1}	0.47	R	0.9981	R	0.9943		
		A_{approx}/%	2.3	A_{approx}/%	4.5		

molecules.[44] Therefore, isoelectric point of protein mostly depends on the applied method.[46]

Kinetic Study of the Silver Binding Process. Kinetics of the silver cations sorption onto lactoferrin is depicted in Figure 4 as the plot of the change of silver ions' concentration in solution per unit time. It may be observed that the decrease of the silver concentration is not a linear process and three separate segments were identified: (i) initial rapid sorption step, (ii) gradual sorption step, and (iii) sorption equilibrium. The sorption in the first step was very fast (the first 4 min) and during this time about 60% of the silver ions were removed by lactoferrin. The sorption capacity of lactoferrin during the first step was 6.58 mg g^{-1}. The sorption in the second step is considerably slower and ends in 20 min from the beginning of the sorption process. During the second step, sorption effectiveness increased up to 73.6% and adsorption up to 8.1 mg/g. After the second step, the sorption process attains equilibrium. The rate constants of the silver sorption kinetics were calculated for the linear segments of the first two steps applying the zero order kinetic model. It can be concluded that the speed of the sorption process is of the order higher in initial first step compared with the second step of the silver sorption.

The results of the fitted kinetics from the nonlinear pseudo-first-order and the pseudo-second-order kinetics models are shown in Figure 4. The calculated kinetic constants are summarized in Table 3. Values of the statistical metrics: correlation coefficient (R), standard deviation (S) and relative approximation error (A_{approx}) have shown that kinetics of the silver ions sorption by lactoferrin should be more accurately described with the pseudo-first-order kinetics model. The obtained kinetic data were tested against the Weber−Morris intraparticle diffusion model in respect to identify the involved mechanisms of the kinetics sorption. The Weber−Morris plot, i.e., functional dependence between the silver sorption and $t_{0.5}$ is depicted in Figure 4.

The presence of three steps of the sorption process can be observed. The first, initial sharper step, should be attributed to boundary layer diffusion effects, external surface sorption or reduction process of silver ions. The second linear step is due to the gradual adsorption with rate-limiting intraparticle diffusion mechanism. The final step is the equilibrium of the sorption process. The y-axis intercept of the second step line provides the measure of the thickness (volume) of the external surface sorption, while its slope determines the value of the intraparticle diffusion coefficient for the silver sorption by lactoferrin (Table 3). On the basis of characteristics of this plot we may conclude that the sorption process is mainly determined by silver sorption on the external surface of lactoferrin globules. Gradual sorption of silver in the second step indicates that the silver ions diffuses and are absorbed into globule structure of the lactoferrin. The values of the distribution coefficient (K_d) and the change in Gibbs free energy ($-\Delta G_0$) of the silver sorption by lactoferrin were calculated and equal to 699.83 and −16.06 kJ mol^{-1}, respectively. The negative values of Gibbs free energy indicate the spontaneous nature of the sorption processes for binding of silver to lactoferrin.

Spectroscopic Study of the Silver Binding Process. Spectral characteristics of native and modified lactoferrin were determined to find active chemical groups involved in the silver-binding process. Figure S2 illustrates that FTIR spectra derived from silver-enhanced lactoferrin are considerably different than those originating from the native protein (Figure S2A). Differences were observed between the spectra registered at times of 5 min (Figure S2B) and 20 min (Figure S2C). The change is especially evident at 20 min (Figure S2C), i.e., after initialization of the proper silver-binding process to active functional groups of LTF. The infrared range 1650−1400 cm^{-1} was affected by silver binding, and additional bands were manifested. The absorption bands at 1649.17 cm^{-1} (1) in native LTF are a consequence of the presence of amide I vibrations arisen mainly from the C═O stretching vibration,[47−49] whereas amide II region (N−H bending and C−N stretching) occurred at 1544.46 cm^{-1} (2).[47,50] The spectral bands at 1658.39 cm^{-1} (4) and 1659.40 cm^{-1} (11) in silver enhanced LTF indicate antisymmetric stretching vibration from arginine residues, $\nu_{as}(CN_3H_5^+)$.[47,50] This amino-acid constitutes about 5.66% (39) of total number of residues (689) in bovine lactoferrin[51,52] and the FTIR spectra suggest that it is involved in the process of silver binding as additional absorption peaks at 1639.95 cm^{-1} (5), 1649.45 cm^{-1} (12) and 1641.50 cm^{-1} (13) are visible.[53] The bands at 1628.55 cm^{-1} (6) in Ag-LTF (5 min) and 1628.23 cm^{-1} (14) in Ag-LTF (20 min) which are not present in the spectrum of native LTF could be attributed to asymmetric in plane bending vibration from lysine, $\delta_{as}(NH_2)$.[47] Lysine is the third most frequently occurred amino-acid (7.84%) in bovine lactoferrin, and the pK_a value of side chain amino group suggests possible coordination interaction between silver ions and their pair electron.[51] Furthermore, change in spectrum band at range 1560−1565 cm^{-1} indicates the presence of glutamic and aspartic acid $\nu_{as}(COO^-)$ in the protein structure. There are 40 glutamic and 36 aspartic acid residues in a single lactoferrin molecule.[51] The bands at 1562.36 cm^{-1} (7) in Ag-LTF (5 min) and 1564.58 cm^{-1} (15) in Ag-LTF (20 min) originate from deprotonated carboxyl groups and indicate participation in binding of silver cations by glutamic and aspartic acids.[47] The absorption peaks localized at 1548.26 cm^{-1} (8), 1547.34 cm^{-1} (16), 1534.74 cm^{-1} (17) and 1515.51 cm^{-1} (18) are related to amide II vibrations. The intensity of the peak 1502.14 cm^{-1} (9) suggests the presence of Tyr−O$^-$ with stretching ν(C═C) and in plane bending vibrations δ(C−H).[53] Tyrosine contributes to 3.19% of total amino-acid residues of Lf.[51] The spectral band at 1465.25 cm^{-1} (10) could originate from in plane bending of methylene (CH_2) group. Finally, the band at 1440.40 cm^{-1} (19) is characteristic for His$^-$ as well as bending from methyl (CH_3) group and stretching from CN group.[47] Histidine is a rare amino-acid in lactoferrin and constitutes only 1.31%[51,52] of

DOI: 10.1021/jacs.6b02699
J. Am. Chem. Soc. 2016, 138, 7899−7909

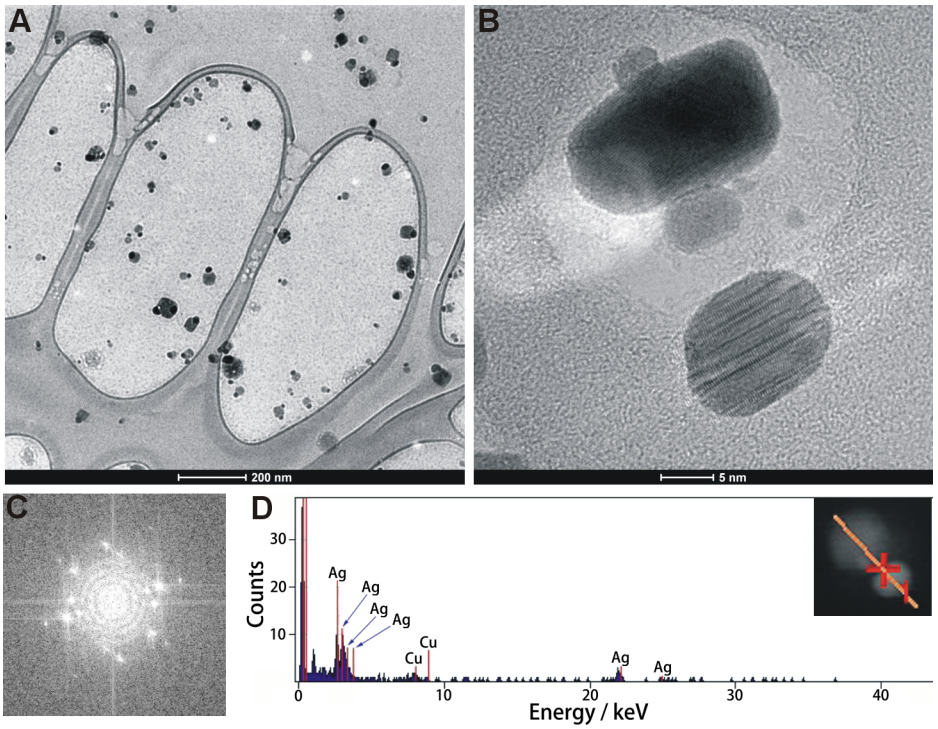

Figure 5. TEM image of Ag-LTF nanocomplexes. Bar: (A) 200 nm, (B) 5 nm, (C) FFT, and (D) EDX spectra.

total LTF residues. The change at spectra range 1440−1465 cm^{-1} could indicate the contribution of imidazole and phenolic ring in sandwich binding of silver ions by Lf.

Another technique used to understand the silver-binding mechanism to lactoferrin was Raman spectroscopy. In Figure S3A a compilation of four Raman spectra in broad range of 100−1900 cm^{-1} is depicted. The first comes from native protein and the three remaining originate from complexes of lactoferrin with silver cations after 2, 3, and 20 min of ongoing reaction (Figure S3). The spectral bands at 238 cm^{-1} (1), 261 cm^{-1} (2) and 292 cm^{-1} (3) could originate from sulfur-containing residues such as cysteine.[54,55] In lactoferrin: 34 out of total 689 residues correspond to cysteine.[51] The signals at 480 cm^{-1} (4) and 593 cm^{-1} (5) could also originate from this amino-acid.[55] Tryptophan could be involved in silver binding because of the absorption peak at 639 cm^{-1} (6), whereas C−S stretching from cysteine, cystine or methionine is observable at 681 cm^{-1} (7), 742 cm^{-1} (8) and 780 cm^{-1} (9).[54] Tyrosine doublet is noticeable at 837 cm^{-1} (10) and 846 cm^{-1} (11).[55] Tyrosine is an amino-acid with moderate frequency of occurrence (3.19%) in lactoferrin.[51] The absorption peak localized at 950 cm^{-1} (12) could indicate α-helix vibration.[48] Phenylalanine is amino-acid found at 1005 cm^{-1} (13) and represented in Lf by 22 residues of this type.[54−56] In Figure S3B, a comparison of 13 peaks (Raman shift 100−1000 cm^{-1}) is depicted. Within this narrow spectrum range there are no differences in abundance and localization of bands between all four presented spectra. However, a considerable change was observed for the spectral band 1088 cm^{-1} (14) (Figure S3C). It occurs only in spectra after 20 min of silver binding reaction and is not seen in the remaining spectra. The band at 1109 cm^{-1} (15) could be attributed to tyrosine residues.[54] Several bands from range 1140−1220 cm^{-1} could originate from tryptophan, tyrosine or phenylalanine residues.[54−56] Amide III region occurred at 1250 cm^{-1} (19). Tryptophan is a possible source of the four following peaks: 1308 cm^{-1} (20), 1340 cm^{-1} (21), 1362 cm^{-1} (22) and 1526 cm^{-1} (24). The signal from 1451 cm^{-1} (23) is related to in plane bending vibrations of methylene (CH_2) groups.[51,55] The peak localized at 1596 cm^{-1} (25) is believed to originate from NH_3^+ group of lysine.[54] Importantly, in Figure S3D and Figure S3E shifts of peaks 1340 cm^{-1} (21), 1451 cm^{-1} (23) and 1526 cm^{-1} (24), can be observed. They occur only after the 20 min of ongoing reaction. Neither shifts nor appearance of additional signals are observable for the other spectra.

Transmission Electron Microscopy (TEM) Imaging. TEM analysis revealed that metallic silver is present in the sample (Figure 5). Silver nanocomplex exhibited a characteristic double spherical shape (Figure 5A, 5B). Interplanar spacing of created nanoparticles lattice was approximately 0.23 nm which is typical for silver (Figure 5C).[57] Intense signals revealed the presence of elemental silver. EDX spectra (Figure 5D) of Ag-LTF confirmed that silver was the major element with a signal of approximately 3 keV.[58] The detected amounts of C, O, S and P could be assigned to the organic compounds of proteins attached to the silver nanoparticles. Copper signals correspond to the TEM grid. Particle size distribution (PSD) was in a range of 8−18 nm with average value of 13 ± 5 nm.

Molecular Dynamics and Quantum Mechanics (QM) Studies of Silver Binding onto/into Lactoferrin. Molecular dynamics (MD) analysis was performed in order to complement the experimental results detailing the mechanism of binding of silver cations to bovine lactoferrin (LTF), and pinpoint their binding sites. Snapshots were sampled every 0.01 ns. Silver ions were deemed bound to active centers of LTF if the distance between the center of Ag^+ cation and the binding site was no further than 0.25 nm. The number of bound ions was measured for each sampled snapshot. Finally, the average number of ions was computed for all the MD snapshots. It was found that on average two silver cations were bound to LTF

DOI: 10.1021/jacs.6b02699
J. Am. Chem. Soc. 2016, 138, 7899−7909

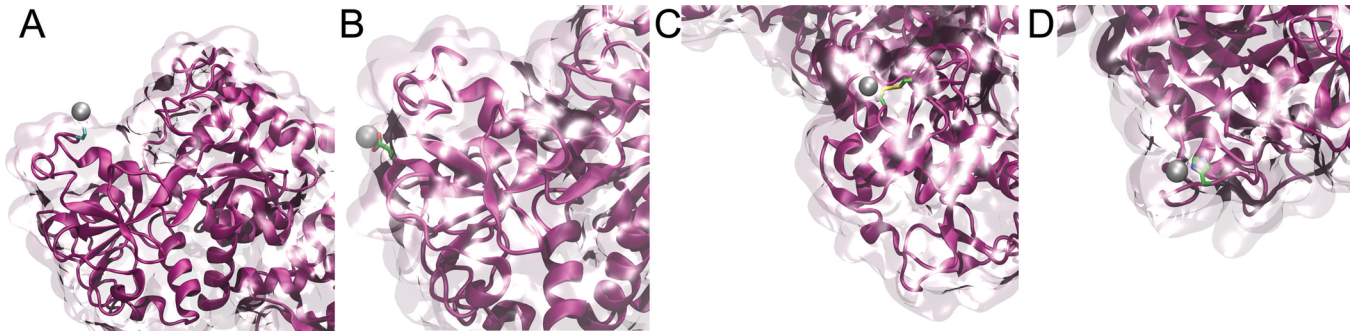

Figure 6. The structures of Ag-LTF complex. Silver cations bound to (A) glutamic acid, (B) aspartic acid, (C) cysteine and (D) histidine. Representation of the protein follows that of Figure 1. Silver cations are represented by gray spheres, while the potential binding sites are represented by sticks with different colors for atoms (carbon: green, oxygen: red, nitrogen: blue, sulfur: yellow).

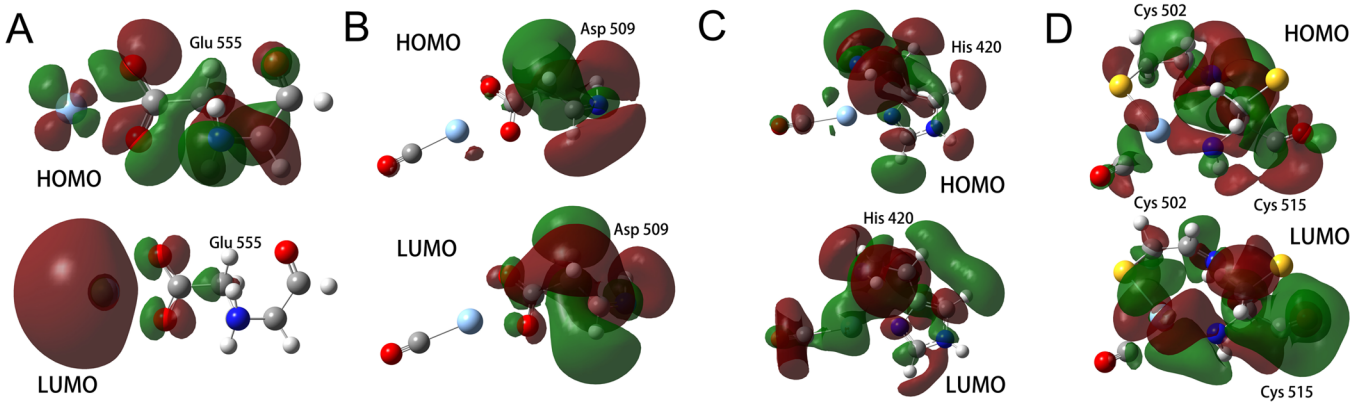

Figure 7. Localization of highest occupied (HOMO) and lowest unoccupied (LUMO) molecular orbitals (MOs) for Ag^+ bound to carboxyl groups of (A) Glu 555, (B) Asp 509, (C) imidazole ring of His 420, and (D) thiol group of Cys 502. Positive segments of MOs are depicted in red, whereas their negative segments are depicted in green color. Atoms are represented in different colors (carbon: gray, silver: light blue, nitrogen: dark blue, oxygen: red, hydrogen: white, and sulfur: yellow).

(Figure S4). Experimental value of cumulative maximum sorption capacity of the initial adsorption kinetic segment was five silver atoms per one lactoferrin molecule, whereas for the second slower intraparticle diffusion segment it was six silver atoms per one lactoferrin molecule (detailed calculation in Supporting Information).

Extrapolating the average number of bound silver ions obtained by MD analysis to the macroscopic scale, it was computed that 50% of silver was bound to LTF, whereas the rest corresponds to reduced or crystallized form of silver.

On the other hand, six amino-acid residues were found to be directly or indirectly involved in interaction with silver: glutamic acid (Glu), aspartic acid (Asp), cysteine (Cys), histidine (His), arginine (Arg), and lysine (Lys). Glu, Asp, Cys and His are directly, whereas Arg and Lys are indirectly involved in binding of lactoferrin. The structures of lactoferrin, with Ag^+ ions bound to its surface are depicted in Figure 6. It can be observed that the silver cation is coordinated with several amino-acids: Glu 555 (Figure 6A) and Asp 509 (Figure 6B) which are the dominant residues for binding. Other residues involved in silver binding were Arg 570 and Lys 441 (Figure S5A), Cys 502 (Figure 6C), as well as His 420 (Figure 6D).

The identified binding sites involved in direct binding of silver correspond to four amino-acids (Cys, His, Glu and Asp) that most often bind metal ions,[59,60] because atoms of their polar or charged side chains can coordinate them. Results of the MD analysis complements the spectroscopic experimental findings well, where the IR bands at 1562.36 cm^{-1} (7) in Ag-LTF (5 min) and 1564.58 cm^{-1} (15) (Figure S2B) in Ag-LTF (20 min, Figure S2C) originate from deprotonated carboxyl groups, which indicates participation of glutamic and aspartic acid in binding of silver cations.[47] Even though the silver cation was coordinated with the carboxyl group of Glu 567, its presence in the environment of Arg 570 and Lys 441 is the reason for the shifts in their IR and Raman peaks, respectively (see Experimental Section: spectroscopic study of the silver binding process).

Results of the MD analysis have shown that the silver cation was bound to the thiol (C-SH) group of Cys 502 which complements the experimental results where the Raman stretching of C−S at 681 cm^{-1} (6)[53] exhibited a shift for the Ag-LTF complex.

It was also shown that the silver cation was bound to the nitrogen of the imidazole ring of His 420. This complements the experimental FTIR findings where spectra in the range 1440−1465 cm^{-1} characteristic for histidine[47] exhibit a change.

Density functional theory (DFT) QM calculations were performed for three of the identified binding sites. Namely, three separate simulations were performed: (i) Ag^+ and Glu 555 (Figure 7A), (ii) Ag^+ and Asp 509 (Figure 7B), (iii) Ag^+ and His 420, as well as (iv) Ag^+ and Cys 502 forming disulfide bond with Cys 515 (Figure 7C) in order to support the reduction of silver cations after sorption to binding sites of LTF.

DOI: 10.1021/jacs.6b02699
J. Am. Chem. Soc. 2016, 138, 7899−7909

Oxidation and/or reduction reactions occur due to the exchange of electrons in frontier molecular orbitals (HOMO/LUMO) of the interacting species. Since these kinds of attractive interactions occur between the occupied MO of one species and unoccupied MO of the other,[61] their localization is useful in approximating them.

It can be observed from Figure 7A that the HOMO orbitals are largely localized on Glu 555 indicating its oxidation, while LUMO orbitals are dominantly localized on the silver indicating its reduction. On the other hand, there is no observable oxidation or reduction between the silver cation and Asp 509 (Figure 7B). The silver is only coordinated with Asp 509. Analogous to Glu 555, Glu 567 exhibited strong localization of HOMO orbitals indicating oxidation, whereas the LUMO orbitals are largely localized on Glu 567 indicating reduction (Figure S5B). Proteins are also able to bind nanoparticles either through free amine groups, imidazole ring or thiol groups. They form the coating covering the particles which prevent their agglomeration and ensure the stability of the silver nanoparticles.[62] In the case of silver binding to His 420, there is no clear indication of oxidation of amino-acids or reduction of silver (Figure 7C). There is however observable mixing of HOMO and LUMO orbitals indicating binding between the silver and the imidazole ring of His 420. Active carbonyl groups of enzymes are also commonly responsible for the reduction process of silver ions in biological systems.[63] Here, it was found that the silver cation has broken the disulfide bond between Cys 502 and 515, and bound to the thiol group of Cys 502 due to the interaction of their frontier orbitals (Figure 7D). Several electrophiles, such as the silver cation possess the ability to reversibly break disulfide bonds in proteins cleaving the disulfide into individual thiol groups.[64] From Figure 7D it can be observed that the LUMO orbitals are strongly concentrated on the Ag+ cation and Cys 505 and 515, whereas the HOMO orbitals are strongly concentrated only on the amino acids. Mixing of HOMO and LUMO orbitals of two cysteine residues indicates a broken disulfide bond. The initiated reduction process occurs by electron transfer from amino-acids' residues of LTF to the adsorbed silver cations giving rise to atomic silver (Ag^0) which was confirmed by DFT calculations. In the following step, the reduced silver (Ag^0) plays a role of nucleation sites where silver cations (Ag^+) are reduced to atomic silver by an electrochemical process that lead to the formation of silver nanoclusters (Ag^0_n).[65] These nanoclusters are subject to coalescence and creation of nanoparticles stabilized by protein molecules. Moreover, it was reported that the creation of silver nanoparticles onto peptides is a spontaneous process, without requiring adding a reducing agent.[66]

Finally, synthesized Ag-LTF complexes are heterogeneous in nature. In the first rapid stage of reaction, lactoferrin clusters are formed, while active centers on their surface such as deprotonated carboxyl groups of Glu and Asp, are responsible for sorption, reduction and crystallization process of silver nanoparticles.They were the dominant amino-acids for silver binding, i.e., throughout the simulation 44.08 and 38.84% of binding sites were Glu and Asp, respectively. The third most abundant binding site was the carbonyl (C═O) group of amino-acids' backbone (16.92%). For illustration Ag^+ binding to backbone of His is depicted in Figure S6. This result complements the experimental spectral findings where a major peak (1) at 1649.17 cm^{-1} (Figure S2A) corresponding to the carbonyl group stretching[47−49] (in native LTF) exhibits a change after both 5 (Figure S2B) and 20 min (Figure S2C) of ongoing binding reaction.

In the second, considerably slower stage of silver binding, system is aimed at equilibrium. The rest of unreduced silver ions are bound to free functional groups of lactoferrin, and possibly create the modified electrostatic motifs, e.g., $[Asp^-]$-$[Ag^+]$, $[Glu^-][Ag^+]$ and $[His^-][Ag^+]$. Here, silver cations are diffused into the lactoferrin clusters, but they are still bound to surfaces of LTF proteins buried in them. Since silver has a stable coordination between two imizadole rings of two His residues in their neutral form,[67] we hypothesize that this binding occurs in the second stage of the reaction where Ag^+ ions diffuse into LTF clusters, and form the bond between two histidine residues of two distinct LTF molecules: (LTF)His-Ag-His(LTF). In comparison with previously reported studies,[9−13] in this work the nature of silver binding to lactoferrin was described. The obtained results give impact to understanding the complex uptake mechanism of metal ions by a protein.

Antibacterial Activity of Silver-Lactoferrin Complexes. To compare antibacterial activity of LTF and complex Ag-LTF we used measurements of optical density, zones of inhibition and direct counting of silver and dead cells with flow cytometer. Optical density allows for estimation of the concentration of bacterial cells in a liquid. Our studies showed that after treatment with the Ag-LTF complex, optical density of all tested bacteria strains (*E. faecalis*, *E. coli*, P. *aeruginosa*, MRSA and *S. aureus*) was lower than in the control sample which suggests that obtained complexes limits their growth. However, after adding only LTF, value of optical density was similar to the control sample which indicates that this agent does not exhibit significant antibacterial activity. Disc diffusion method confirmed that Ag-LTF complex can act as a germ-destroying agent. Zones of inhibition were visible around discs that had the highest concentrations of Ag-LTF (25 and 50 μg/mL). The most susceptible strains of bacteria were MRSA, *S. aureus* and *E. faecalis* with average zones of inhibition of 35, 25, and 28 nm, respectively. However, LTF alone, even at a concentration of 50 μg/mL did not create any zone of inhibition which indicates that this protein does not display germicidal activity against tested bacteria strains on its own.

Flow cytometry was applied to evaluate the inhibitory effects of LTF and Ag-LTF complex at different concentrations (0, 12.5, 25, and 50 μg/mL). The total counts of live and dead cells not treated and treated with LTF and Ag-LTF are presented in Table S1. Studies showed that for strains such as *E. faecalis*, *E. coli*, MRSA and *S. aureus*, LTF at concentration 50 μg/mL and below does not display antibacterial activity. In case of MRSA and *S. aureus* number of cells was even slightly higher in samples with added LTF than in control samples. Only *P. aeruginosa* was susceptible to LTF and concentration at 50 μg/mL inhibited its growth in 75.7%. LTF is generally recognized as protein with antibacterial properties. In our study this protein did not inhibit the growth of most tested bacteria and in some cases even enhanced their viability. We can exclude that this phenomenon may be due to high saturation of purified lactoferrin with iron. Studies showed that iron-saturated lactoferrin stimulates aggregation and biofilm formation.[68,69] Clinical studies on human subjects showed that antibacterial activity of LTF purified from saliva depends on single nucleotide polymorphism (SNP) that produces a shift from arginine to lysine at amino-acid residue 47 in LTF antimicrobial agent. We can also rule out that in our case the

DOI: 10.1021/jacs.6b02699
J. Am. Chem. Soc. 2016, 138, 7899−7909

lack of antibacterial activity is associated with genotype differences.

However, complex Ag-LTF appeared to be effective against all studied strains. *P. aeruginosa*, *S. aureus* and MRSA were especially susceptible and the lowest used concentration, i.e., 12.5 μg/mL inhibited growth of 86.3%, 66% and 74.3% of *P. aeruginosa*, *S. aureus* in and MRSA, respectively. However, concentration at 50 μg/mL limited the growth of 98.7% of *P. aeruginosa* and more than 97% of *S. aureus*. In this sample an especially high number of dead cells (88.52%) was noticed. Similar results were obtained for MRSA, where this concentration of Ag-LTF complex reduced viability almost completely (99.5%) and the number of dead cells increased to 70.55%. High percent of dead cells was also present in samples of *E. faecalis* even in the lowest used concentration of the complex (81.14%). These results suggest that complex of silver and lactotransferrin kills bacteria and can be classified into a group of bactericides. Less susceptible to Ag-LTF was *E. coli*, where the concentration of 12.5 μg mL^{-1} did not considerably reduce the viability of the bacterial cells. Only higher concentrations, i.e., 25 and 50 μg mL^{-1} inhibited the growth in ca. 67%, and at this time the number of dead cells increased to almost 80%. In order to verify whether the Ag-LTF complex is as effective as commercially available antibiotics, we compared total counts of live and dead cells after treatment with antibiotics and Ag-LTF (Table S2). We selected antibiotics that are very effective in controlling particular bacterial strain as well as those which probably exhibit only weak antibacterial activity against selected bacteria strains. *P. aeruginosa* is a strain of bacteria which is resistant to a large range of antibiotics. In our study, complex Ag-LTF at a concentration of 50 μg mL^{-1} was as effective as cefotaxime which is normally used to treat *P. aeruginosa* infections. Both agents inhibited its growth more than 97%. Ag-LTF complex at a concentration of 12.5 μg mL^{-1} was considerably more effective than clinadmycin (86.3% and 33.00% inhibition, respectively). For MRSA, the efficacy of Ag-LTF (50 μg mL^{-1}, 99.5%) was comparable with efficiency of clindamycin (92.68%) and metronidazole (93.4%). For *E. coli* combination of amoxicillin and clavulanic acid has similar antibacterial activity as Ag-LTF complex (over 60%). Antibacterial activity of obtained Ag-LTF complexes was also comparable with activity of silver nanoparticles biologically synthesized by new *Actinomycetes CGG 11n* strain measured in the experiment conducted in similar conditions.[37] Only for *P. aeruginosa*, Ag-LTF at a concentration 12.5 μg mL^{-1} was much more effective than silver nanoparticles at the same concentration (86.34% of inhibition for Ag-LTF in compare to ca. 20% for silver nanoparticles).

These results indicate that antibacterial activity of the Ag-LTF complex is comparable with commercially available antibiotics. Particularly promising is the possibility of application of obtained complexes in treatment of infections caused by multidrug resistant bacteria such as *P. aeruginosa*.

CONCLUSIONS

Present study manifested evidence that the silver ions should be effectively uptaken by native forms of LTF from an aqueous solution. Kinetics of the silver binding to the protein is a heterogeneous process that involved two main stages: (i) internal diffusion and sorption onto external surface of lactoferrin globules; (ii) internal diffusion and binding into lactoferrin globule structure. Formation of the silver nanoparticles was spontaneously initiated in the first stage with fast binding of silver ions to glutamic and aspartic acid on the surface of LTF clusters. In the second stage of the reaction, silver ions diffused into the LTF clusters and bound onto active groups of lactoferrin (formation of true silver-proteins), e.g., silver-mediated binding of individual LTF proteins: (LTF)His-Ag-His(LTF) bond. Potential binding sites were pinpointed using molecular dynamics (MD) simulations, which were consistent with the experimental findings. Furthermore, the reduction of silver was confirmed by simulating the identified binding sites using density functional theory. Aspartic and glutamic acid were found to be the dominant amino-acids for binding of silver cations in the form of sorption and their consequent reduction.

Results of the antibacterial activity study prospectively suggest that synthesized silver-lactoferrin could be used in the field of medicine and food industry as innovative, economically and environmentally feasible antimicrobial agent.

ASSOCIATED CONTENT

Supporting Information

The Supporting Information is available free of charge on the ACS Publications website at DOI: 10.1021/jacs.6b02699.

One-dimensional electropherogram of lactoferrin. Fourier transform-infrared and Raman spectra for native lactoferrin (LTF), and Ag-LTF nanocomplexes. Summary of antimicrobial activity of Ag-LTF nanocomplexes and commercial antimicrobial agents against known pathogens. Calculation procedure of the number of silver atoms per one lactoferrin molecule. Histogram depicting the frequency of the number of bound silver ions to LTF, sampled every 0.01 ns of ongoing MD simulation. Molecular structures of lactoferrin with the silver cation bound to glutamic acid in the environment of arginine and lysine, and the silver cation bound to the carbonyl group of His backbone. (PDF)

AUTHOR INFORMATION

Corresponding Author

*bbusz@chem.umk.pl

Notes

The authors declare no competing financial interest.

ACKNOWLEDGMENTS

This work was financially supported by the National Science Centre in the frame of the project Symfonia 1 No. 2013/08/W/NZ8/701 (2013-2016), Maestro 6, No. 2014/14/A/ST4/00641 (2015-2017) and Preludium 2013/11/N/ST4/01835. The work was additionally supported by the Pukyong National University and Brain Busan 21 project grants for 2015/2016.

REFERENCES

(1) Sánchez, L.; Calvo, M.; Brock, J. H. *Arch. Dis. Child.* **1992**, *67*, 657−61.
(2) Levay, P. F.; Viljoen, M. *Haematologica* **1995**, *80*, 252−267.
(3) Adlerova, L.; Bartoskova, A.; Faldyna, M. *Vet. Med. Czech* **2008**, *53*, 457−468.
(4) Tsuda, H.; Sekine, K.; Fujita, K.; Ligo, M. *Biochem. Cell Biol.* **2002**, *80*, 131−136.
(5) Kalaiselvi, A.; Gantz, S.; Ramalingam, C. *Int. J. Pharm. Pharm. Sci.* **2013**, *5*, 274−277.

DOI: 10.1021/jacs.6b02699
J. Am. Chem. Soc. 2016, 138, 7899−7909

(6) Railean-Plugaru, V.; Pomastowski, P.; Wypij, M.; Szultka-Młyńska, M.; Rafińska, K.; Golińska, P.; Dahm, H.; Buszewski, B. *J. Appl. Microbiol.* **2016**, *120*, 1250−1263.
(7) Vrček, I. V.; Zuntar, I.; Petlevski, R.; Pavičić, I.; Dutour Sikirić, M.; Ćurlin, M.; Goessler, W. *Environ. Toxicol.* **2016**, *31*, 679.
(8) Jung, W. K.; Koo, H. C.; Kim, K. W.; Shin, S.; Kim, S. H.; Park, Y. H. *Appl. Environ. Microbiol.* **2008**, *74*, 2171−2178.
(9) Mulley, G.; Jenkins, A. T.; Waterfield, N. R. *PLoS One* **2014**, *9*, 1−9.
(10) Wei, H.; Wang, Z.; Zhang, J.; House, S.; Gao, Y. G.; Yang, L.; Robinson, H.; Tan, L. H.; Xing, H.; Hou, C.; Robertson, I. M.; Zuo, J. M.; Lu, Y. *Nat. Nanotechnol.* **2011**, *6*, 93−97.
(11) Wei, H.; Lu, Y. *Chem. - Asian J.* **2012**, *7*, 680−683.
(12) Lee, Y.; Kim, J.; Yun, D. S.; Nam, Y. S.; Shao-Horn, Y.; Belcher, A. M. *Energy Environ. Sci.* **2012**, *5*, 8328−8334.
(13) Pazos, E.; Sleep, E.; Pérez, C. M. R.; Lee, S. S.; Tantakitti, F.; Stupp, S. I. *J. Am. Chem. Soc.* **2016**, *138*, 5507−5510.
(14) Pomastowski, P.; Walczak, J.; Gawin, M.; Bocian, S.; Piekoszewski, W.; Buszewski, B. *Anal. Methods* **2014**, *6*, 5236−5244.
(15) Ho, Y. S.; McKay, G. *Process Biochem.* **1999**, *34*, 451−456.
(16) Cheung, C. W.; Porter, J. F.; McKay, G. *Water Res.* **2001**, *35*, 605−612.
(17) Weber, W. J.; Morris, J. C. *J. Sanit. Eng. Div., Am. Soc. Civ. Eng.* **1963**, *89*, 31−60.
(18) Moore, S. A.; Anderson, B. F.; Groom, C. R.; Haridas, M.; Baker, E. N. *J. Mol. Biol.* **1997**, *274*, 222−236.
(19) Humphrey, W.; Dalke, A.; Schulten, K. *J. Mol. Graphics* **1996**, *14*, 33−38.
(20) Phillips, J. C.; Braun, R.; Wang, W.; Gumbart, J.; Tajkhorshid, E.; Villa, E.; Chipot, C.; Skeel, R. D.; Kale, L.; Schulten, K. *J. Comput. Chem.* **2005**, *26*, 1781−1802.
(21) Best, R. B.; Zhu, X.; Lopes, P. E. M.; Mittal, J.; Feig, M.; MacKerell, A. D., Jr. *J. Chem. Theory Comput.* **2012**, *8*, 3257−3273.
(22) Won, Y. *J. Phys. Chem. A* **2012**, *116*, 11763−11767.
(23) Zoete, V.; Cuendet, M. A.; Grosdidier, A.; Michielin, O. *J. Comput. Chem.* **2011**, *32*, 2359−2368.
(24) Roy, A.; Zhang, Y. *Nucleic Acids Res.* **2012**, *40*, W471−W477.
(25) Karthikeyan, S.; Yadav, S.; Paramasivam, M.; Srinivasan, A.; Singh, T. P. *Acta Crystallogr., Sect. D: Biol. Crystallogr.* **2000**, *56*, 684−689.
(26) Kumar, P.; Yadav, S.; Singh, T. P. *Indian J. Biochem. Biophys.* **2002**, *39*, 16−21.
(27) Sharma, A. K.; Kumar, S.; Sharma, V.; Nagpal, A.; Singh, N.; Tamboli, I.; Mani, I.; Raman, G.; Singh, T. P. *Proteins: Struct., Funct., Genet.* **2001**, *45*, 229−236.
(28) Darden, T.; Perera, L.; Li, L.; Pedersen, L. *Structure* **1999**, *7*, R55−R60.
(29) Kubo, R.; Toda, M.; Hashitsume, N. *Statistical Physics II: Nonequilibrium Statistical Mechanics*; Springer-Verlag: Berlin, 1991.
(30) Hohenberg, P.; Kohn, W. *Phys. Rev.* **1964**, *136*, B864−B871.
(31) Kohn, W.; Sham, L. J. *Phys. Rev.* **1965**, *140*, 1133−1138.
(32) Yanai, T.; Tew, D.; Handy, N. *Chem. Phys. Lett.* **2004**, *393*, 51−57.
(33) Rassolov, V. A.; Ratner, M. A.; Pople, J. A.; Redfern, P. C.; Curtiss, L. A. *J. Comput. Chem.* **2001**, *22*, 976−984.
(34) Hay, P. J.; Wadt, W. R. *J. Chem. Phys.* **1985**, *82*, 270−283.
(35) Wadt, W. R.; Hay, P. J. *J. Chem. Phys.* **1985**, *82*, 287−298.
(36) Hay, P. J.; Wadt, W. R. *J. Chem. Phys.* **1985**, *82*, 299−310.
(37) Railean-Plugaru, V.; Pomastowski, P.; Rafinska, K.; Kupczyk, W.; Jackowski, M.; Buszewski, B. *Electrophoresis* **2016**, *37*, 752−761.
(38) Leclercq, G.; Gengler, N.; Soyeurt, H.; Bastin, C. *Livest. Sci.* **2013**, *151*, 158−162.
(39) Kuczynska, B.; Puppel, K.; Gołebiewski, M.; Metera, E.; Sakowski, T.; Słoniewski, K. *J. Sci. Food Agric.* **2012**, *92*, 2899−2904.
(40) Ye, X. Y.; Nishimura, T.; Yoshida, S. *Biosci., Biotechnol., Biochem.* **1997**, *61*, 782−786.
(41) Brock, J. H.; Arzabe, F.; Lampreave, F.; Piñeiro, A. *Biochim. Biophys. Acta, Protein Struct.* **1976**, *446*, 214−225.
(42) Šlechtová, T.; Gilar, M.; Kalíková, K.; Tesařová, E. *Anal. Chem.* **2015**, *87*, 7636−7643.
(43) Salgın, S.; Salgın, U.; Bahadır, S. *Int. J. Electrochem. Sci.* **2012**, *7*, 12404−12414.
(44) Pomastowski, P.; Sprynskyy, M.; Buszewski, B. *Colloids Surf., B* **2014**, *1*, 121−127.
(45) Shimazaki, K.; Kawano, N.; Yoo, Y. C. *Comp. Biochem. Physiol.* **1999**, *98*, 417−422.
(46) Bezwoda, W. R.; Mansoor, N. *Biomed. Chromatogr.* **1989**, *3*, 121−126.
(47) Barth, A. *Biochim. Biophys. Acta, Bioenerg.* **2007**, *1767*, 1073−1101.
(48) Haris, P. I.; Severcan, F. *J. Mol. Catal. B: Enzym.* **1999**, *7*, 207−221.
(49) Iafisco, M.; Di Foggia, M.; Bonora, S.; Prat, M.; Roveri, N. *Dalton Trans.* **2011**, *40*, 820−827.
(50) Sreeprasad, T. S.; Maliyekkal, M. S.; Deepti, K.; Chaudhari, K.; Xavier, P. L.; Pradeep, T. *ACS Appl. Mater. Interfaces* **2011**, *3*, 2643−2654.
(51) Steijns, J. M.; van Hooijdonk, A. C. M. *Br. J. Nutr.* **2000**, *84*, 11−17.
(52) Baker, E. N.; Baker, H. M. *Cell. Mol. Life Sci.* **2005**, *62*, 2531−2539.
(53) Barth, A.; Zscherp, C. *Q. Rev. Biophys.* **2002**, *35*, 369−430.
(54) Li-Chan, E. C. Y.; Nakai, S.; Hirotsuka, M. In *Protein Structure-Function Relationships in Foods*; Yada, R. Y., Jackman, R. L., Smith, J. L., Eds.; Blackie Academic & Professional: London, 1994; pp 163−197.
(55) Li-Chan, E. C. Y. *Lait* **2007**, *87*, 443−458.
(56) Iafisco, M.; Foltran, I.; Di Foggia, M.; Bonora, S.; Roveri, N. *J. Therm. Anal. Calorim.* **2011**, *103*, 41−47.
(57) Tamuly, C.; Hazarika, M.; Bordoloi, M.; Das, M. R. *Mater. Lett.* **2013**, *1*, 102−103.
(58) Elavazhagan, T.; Arunachalam, K. D. *Int. J. Nanomed.* **2011**, *6*, 1265−1278.
(59) Auld, D. S. *BioMetals* **2001**, *14*, 271−313.
(60) Golovin, A.; Dimitropoulos, D.; Oldfield, T.; Rachedi, A.; Henrick, K. *Proteins: Struct., Funct., Genet.* **2005**, *58*, 190−199.
(61) Fukui, K.; Yonezawa, T.; Shingu, H. *J. Chem. Phys.* **1952**, *20*, 722−725.
(62) Sastry, M.; Ahmad, A.; Khan, M. I.; Kumar, R. *Curr. Sci.* **2003**, *85*, 162−170.
(63) Bhat, R.; Deshpande, R.; Ganachari, S. V.; Huh, D. S.; Venkataraman, A. *Bioinorg. Chem. Appl.* **2011**, *2011*, 1.
(64) Creighton, T. E. *BioEssays* **1998**, *8*, 57−63.
(65) Ershov, B. G.; Janata, E.; Henglein, A.; Fojtik, A. *J. Phys. Chem.* **1993**, *97*, 4589−4627.
(66) Polte, J.; Tuaev, X.; Wuithschick, M.; Fischer, A.; Thuenemann, A. F.; Rademann, K.; Kraehnert, R.; Emmerling, F. *ACS Nano* **2012**, *6*, 5791−5802.
(67) Mirolo, L.; Schmidt, T.; Eckhardt, S.; Meuwly, M.; Fromm, K. M. *Chem. - Eur. J.* **2013**, *19*, 1754−1761.
(68) Berlutti, F.; Morea, C.; Battistoni, A.; Sarli, S.; Cipriani, P.; Superti, F.; Ammendolia, M. G.; Valenti, P. *Int. J. Immunopathol. Pharmacol.* **2005**, *18*, 661−670.
(69) Fine, D. H.; Toruner, G. A.; Velliyagounder, K.; Sampathkumar, V.; Godboley, D.; Furgang, D. *Infect. Immun.* **2013**, *81*, 1596−1605.

DOI: 10.1021/jacs.6b02699
J. Am. Chem. Soc. 2016, 138, 7899−7909